Connection of envelope functions at semiconductor heterointerfaces. II. Mixings of Γ and X valleys in GaAs/$Al_xGa_{1-x}As$

T. Ando and H. Akera
Institute for Solid State Physics, University of Tokyo, 7-22-1 Roppongi, Minato-ku, Tokyo 106, Japan
(Received 14 March 1989)

The effective-mass approximation is extended so as to take into account mixings between Γ and X conduction-band valleys at heterointerfaces consisting of $Al_xGa_{1-x}As$ with different x's. Effects of the mixings are included by boundary conditions expressed in terms of a 6×6 interface matrix that gives a set of linear relations among envelope functions and their derivatives at the interface. The interface matrix is calculated in an *sps** tight-binding model with only nearest-neighbor transfer integrals. The intervalley couplings, although not so large, can be represented by two off-diagonal elements of the interface matrix. The usefulness of the present formulation is demonstrated by actual calculations of transmissions and reflections across a single interface and a single barrier structure and also of energy levels in multiple quantum wells. The interface-matrix formalism is extended to treat tunnelings across high barriers to which the envelope-function approximation is not applicable.

I. INTRODUCTION

One typical semiconductor superlattice is made of GaAs/$Al_xGa_{1-x}As$ heterostructures. With the exception of ultrathin layers, low-lying states in the conduction band are localized in the GaAs layer and they are successfully described by the effective-mass approximation if appropriate boundary conditions are imposed at interfaces.[1] In the preceding paper,[2] which will be referred to as I, the boundary conditions have been expressed in terms of a 2×2 interface matrix and calculated in the two relatively simple models, the tight-binding and empirical pseudopotentials. It has been shown that the so-called envelope-function approximation[3–7] (EFA) works surprisingly well in various heterointerfaces including GaAs/$Al_xGa_{1-x}As$, GaSb/InAs, and HgTe/CdTe. The purpose of the present paper is to extend the formalism so as to treat mixings of different conduction-band minima (valleys) at heterointerfaces.

The conduction band of GaAs has two local minima along the [001] direction in the vicinity of X points (called X valleys) as well as the minimum at the Γ point called the Γ valley. On the other hand, AlAs has the lowest minima at the X valleys. At an appropriate Al content in $Al_xGa_{1-x}As$ ($x \sim 0.4$), the Γ and X minima have equal energy. Beyond this critical x, $Al_xGa_{1-x}As$ becomes an indirect-gap material.[8] This direct to indirect transition can occur in GaAs/AlAs quantum wells or superlattices when the thickness of the GaAs layer is sufficiently small. This is because the effective mass of the Γ valley is smaller than that of the X valleys[9] and electrons in the Γ valley are raised higher in energy in comparison with those in the X valleys. Since the energy of X-valley minima is lower in AlAs than in GaAs,[10] the material becomes "spatially" indirect, i.e., the conduction-band bottom changes from the character of the Γ valley in GaAs to that of X valleys in AlAs. A similar transition can be induced by applying high pressures which lower the X-valley energy relative to the Γ valley.

In superlattices grown in the [001] direction, these different Γ and X valleys can couple with each other due to the lack of translational invariance at heterointerfaces. Recently, there has been considerable interest in such mixing effects. Several optical experiments have been performed to study the crossover from direct-Γ-valley to indirect-X-valley conduction-band states[11–21] and some have presented convincing data showing an anticrossing behavior when the energies of Γ and X valleys are sufficiently close.[22] Tunnelings via X-valley states have also been observed in double-barrier structures.[23–28]

There have been reported numerous band-structure calculations in GaAs/$Al_xGa_{1-x}As$ superlattices. Some of the authors performed calculations from first principles,[29–33] and most of the works employed simpler empirical models such as pseudopotentials[34–39] and tight-binding or Wannier orbitals.[40–47] These calculations have demonstrated the crossover from the Γ-like conduction band to the X-like conduction band with decreasing superlattice period in GaAs/AlAs. When these Γ-like and X-like states are close in energy, they repel each other and exhibit small anticrossing. There have been calculations of tunneling probabilities across GaAs/$Al_xGa_{1-x}As$/GaAs single- or multiple-barrier structures using empirical models.[48–55] Such calculations have also demonstrated the presence of mixings of Γ and X valleys at heterointerfaces.

It is highly desirable to extend the effective-mass approximation so as to treat mixings of different valleys at heterointerfaces. In this paper, we propose such an extension of the effective-mass approximation, in which mixings effects are included as boundary conditions for envelope functions at the interface expressed in terms of a 6×6 interface matrix. Further, we extend the interface matrix introduced in I to study tunnelings across high

barriers to which the conventional envelope-function approximation is not applicable.

The paper is organized as follows. In Sec. II a 6×6 interface matrix is introduced and some of its properties are discussed. The interface matrix gives a set of linear relations among envelope functions associated with the Γ valley and those associated with the X valleys at the interface. We assume that the envelope for the Γ valley and those of the X valleys satisfy independent effective-mass equations in bulk. In Sec. III the 6×6 interface matrix is explicitly calculated using an *sps** tight-binding model. Mixings between different valleys are shown to be essentially given by two off-diagonal elements of the interface matrix which are roughly proportional to the difference in the Al content of alloys forming the interface. The resulting interface matrix is used for calculations of tunneling and reflection coefficients at a single interface and a single-barrier structure and for calculations of energy levels in a superlattice in Sec. IV. The interface matrix is applied to a problem of tunnelings across high potential barriers in Sec. V. In this problem, effects of the nonparabolic effective mass play much more important roles than mixings between different valleys. A summary and conclusion are given in Sec. VI. A preliminary account of a part of the work in this paper has been given elsewhere.[56]

II. INTERFACE MATRIX

Let us consider a $GaAs/Al_xGa_{1-x}As$ heterointerface grown in the [001] direction. Throughout this paper we confine ourselves to the case $k_x=k_y=0$, i.e., along the Δ axis. According to various band-structure calculations and experiments, the additional conduction-band minima are now believed to be located slightly away from the X points in GaAs.[57] This is true also in AlAs.[58] Therefore, we have to consider the presence of two inequivalent minima X_+ and X_-, where X_+ and X_- denote the minimum in positive and negative k_z direction, respectively. Figure 1 shows the conduction bands with the Δ_1 symmetry calculated in the *sps** tight-binding model introduced in the next section.

Within the effective-mass approximation,[59] the total wave function is written in the presence of multiple band extrema as

$$\psi(\mathbf{r})\approx\sum_{\alpha}[\psi_\alpha(\mathbf{r})\zeta_\alpha(z)+\psi'_\alpha(\mathbf{r})\nabla\zeta_\alpha(z)]\ , \tag{2.1}$$

with $\nabla=a(\partial/\partial z)$ and a the lattice constant, where $\psi_\alpha(\mathbf{r})$ is the Bloch function at the extremum α and $\psi'_\alpha(\mathbf{r})$ is its first derivative with k_z. Using the usual $\mathbf{k}\cdot\mathbf{p}$ perturbation theory,[59] we have

$$\psi'_\alpha(\mathbf{r})=-ia^{-1}\sum_{j\neq\alpha}\psi_j(\mathbf{r})\frac{\hbar(j|p_z|\alpha)}{m_0(\varepsilon_j-\varepsilon_\alpha)}\ , \tag{2.2}$$

where $\psi_j(\mathbf{r})$ and ε_j are the Bloch function and the energy at the wave vector k_α corresponding to valley α and $(j|p_z|\alpha)$ is the matrix element of the momentum in the z direction. In the bulk, the envelope $\zeta_\alpha(z)$ satisfies the conventional effective-mass equation in the presence of a slowly varying potential:

$$\left[-\frac{\hbar^2}{2m_\alpha}\frac{d^2}{dz^2}+\varepsilon_\alpha+V(z)\right]\zeta_\alpha(z)=E\zeta_\alpha(z)\ . \tag{2.3}$$

That is, the envelopes associated with different extrema are independent of each other in bulk.

The presence of abrupt interface potentials gives rise to mixings between the three different valleys $\alpha=\Gamma$, X_+,X_-. Such mixings can be included as a form of a 6×6 interface matrix $\tilde{T}_{BA}=(\tilde{T}^{\beta\alpha}_{BA})$ as follows:

$$\begin{bmatrix}\zeta^B_\beta(0)\\ \nabla^B_\beta\zeta^B_\beta(0)\end{bmatrix}=\sum_\alpha\tilde{T}^{\beta\alpha}_{BA}\begin{bmatrix}\zeta^A_\alpha(0)\\ \nabla^A_\alpha\zeta^A_\alpha(0)\end{bmatrix}\ , \tag{2.4}$$

where $\tilde{T}^{\beta\alpha}_{BA}=(t^{\beta\alpha}_{ij})$ is a 2×2 matrix, $\nabla^A_\alpha=(m_0/m^A_\alpha)\nabla$, and $\nabla^B_\beta=(m_0/m^B_\beta)\nabla$ with m_0 the free electron mass and m^A_α and m^B_α the effective masses of semiconductors A and B, respectively, at the minimum α.

Such a 6×6 matrix has been calculated previously within the *sps** tight-binding model, the same as that used in the present paper.[60] Unfortunately, applicability of this 6×6 matrix has turned out to be quite limited to the energy range very close to the X-valley minima. The effective mass of the X valleys along the k_z axis is quite large (of the order of the free electron mass) and the energy at wave vector $\pm2\pi/a$ (the Brillouin zone boundaries) is not much different from that of X_+ and X_-. At $k_z=\pm2\pi/a$ the X_+ and X_- valleys interact with each other strongly and the dispersion relation is modified

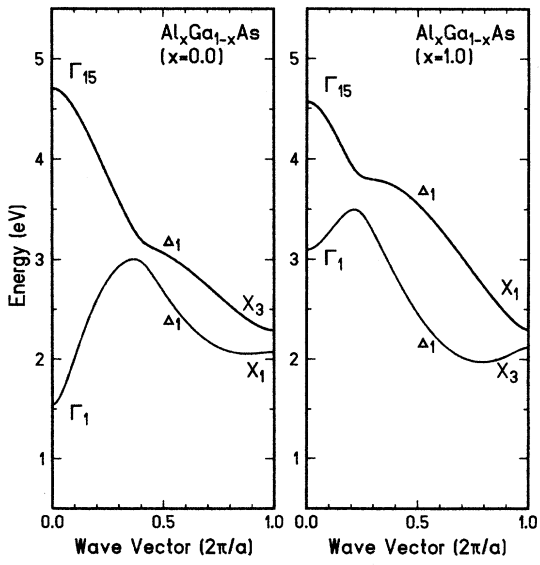

FIG. 1. The energy of the conduction band of GaAs and AlAs as a function of the wave vector in the [001] direction calculated in the *sps** tight-binding model. The energy origin is at the valence-band top at the Γ point.

drastically (see Fig. 1).

We can increase the range of applicability by treating the X valleys as degenerate bands. We choose the X_1 (lower in energy for GaAs and denoted by u) and X_3 (denoted by v) Bloch functions as the basis for the X valleys. The envelopes for the X valleys are given by a vector with two components $\zeta_u(z)$ and $\zeta_v(z)$. By choosing the phase of basis functions appropriately, the envelopes satisfy the following matrix effective-mass equation[59] in the presence of slowly-varying potential $V(z)$:

$$\left[\begin{bmatrix} E_u-(\hbar^2/2m_u)(d^2/dz^2) & i(\hbar^2/2m_0a)P(d/idz) \\ -i(\hbar^2/2m_0a)P(d/idz) & E_v-(\hbar^2/2m_v)(d^2/dz^2)\end{bmatrix}+V(z)-E\right]\begin{bmatrix}\zeta_u\\ \zeta_v\end{bmatrix}=0\ , \tag{2.5}$$

where E_u and E_v are the band energies at the X point, and P is the momentum matrix-element between u and v, i.e., $P=(2a/i\hbar)(u|p_z|v)$. The boundary conditions are still given by Eq. (2.4) except that the valleys are now specified by Γ, u, and v.

We can choose $z=0$ at one of As atomic planes and the phase of the basis Bloch functions such that

$$\psi_\alpha^*=\psi_\alpha \text{ and } \psi_\alpha'^*=\psi_\alpha',\quad \alpha=\Gamma,u,v \tag{2.6}$$

and

$$\begin{aligned}&\psi_\Gamma(-z)=+\psi_\Gamma(z),\quad \psi_\Gamma'(-z)=-\psi_\Gamma'(z)\ ,\\ &\psi_u(-z)=+\psi_u(z),\quad \psi_u'(-z)=-\psi_u'(z)\ ,\\ &\psi_v(-z)=-\psi_v(z),\quad \psi_v'(-z)=+\psi_v'(z)\ .\end{aligned} \tag{2.7}$$

Equation (2.6) shows that all the elements of the 6×6 matrix can be chosen real. Equation (2.7), on the other hand, gives the following relation between $\tilde{T}_{BA}$ and $\tilde{T}_{AB}$, which is the interface matrix of the system obtained by the mirror symmetry operation at $z=0$:

$$\tilde{T}_{AB}=\begin{bmatrix}\sigma_z&0&0\\0&\sigma_z&0\\0&0&-\sigma_z\end{bmatrix}\tilde{T}_{BA}^{-1}\begin{bmatrix}\sigma_z&0&0\\0&\sigma_z&0\\0&0&-\sigma_z\end{bmatrix}, \tag{2.8}$$

where σ_z is the z component of Pauli's spin matrix.

As has been discussed in I and will be shown in the next section, there are cases in which the boundary conditions are written in the same form,

$$W_B\begin{bmatrix}\zeta_\Gamma^B\\ \nabla_\Gamma^B\zeta_\Gamma^B\\ \zeta_u^B\\ \nabla_u^B\zeta_u^B\\ \zeta_v^B\\ \nabla_v^B\zeta_v^B\end{bmatrix}=W_A\begin{bmatrix}\zeta_\Gamma^A\\ \nabla_\Gamma^A\zeta_\Gamma^A\\ \zeta_u^A\\ \nabla_u^A\zeta_u^A\\ \zeta_v^A\\ \nabla_v^A\zeta_v^A\end{bmatrix}, \tag{2.9}$$

both for the case that A is on the left-hand side of the interface ($z<0$) and for the case that A is on the right-hand side. We have the relation $\tilde{T}_{AB}=\tilde{T}_{BA}^{-1}$, which combined with Eq. (2.8) gives

$$\tilde{T}_{BA}=\begin{bmatrix}\sigma_z&0&0\\0&\sigma_z&0\\0&0&-\sigma_z\end{bmatrix}\tilde{T}_{BA}\begin{bmatrix}\sigma_z&0&0\\0&\sigma_z&0\\0&0&-\sigma_z\end{bmatrix}. \tag{2.10}$$

This leads to the following general form of the 6×6 interface matrix:

$$\tilde{T}_{BA}=\begin{array}{c}\\ \zeta_\Gamma\\ \nabla\zeta_\Gamma\\ \zeta_u\\ \nabla\zeta_u\\ \zeta_v\\ \nabla\zeta_v\end{array}\begin{array}{c}\begin{array}{cccccc}\zeta_\Gamma&\nabla\zeta_\Gamma&\zeta_u&\nabla\zeta_u&\zeta_v&\nabla\zeta_v\end{array}\\ \begin{bmatrix}t_{11}^\Gamma&0&t_{11}^{\Gamma u}&0&0&t_{12}^{\Gamma v}\\0&t_{22}^\Gamma&0&t_{22}^{\Gamma u}&t_{21}^{\Gamma v}&0\\t_{11}^{u\Gamma}&0&t_{11}^u&0&0&t_{12}^{uv}\\0&t_{22}^{u\Gamma}&0&t_{22}^u&t_{21}^{uv}&0\\0&t_{12}^{v\Gamma}&0&t_{12}^{vu}&t_{11}^v&0\\t_{21}^{v\Gamma}&0&t_{21}^{vu}&0&0&t_{22}^v\end{bmatrix}\end{array}. \tag{2.11}$$

The flux averaged over a volume of the order of a unit cell is given by

$$\begin{aligned}j(z)&=\frac{\hbar}{2im_0}\left[\psi^*(\mathbf{r})\left[\frac{\partial}{\partial z}\psi(\mathbf{r})\right]-\left[\frac{\partial}{\partial z}\psi^*(\mathbf{r})\right]\psi(\mathbf{r})\right]\\ &\approx\sum_\alpha\frac{\hbar}{2im_\alpha}\left[\zeta_\alpha^*(z)\frac{\partial}{\partial z}\zeta_\alpha(z)-\left[\frac{\partial}{\partial z}\zeta_\alpha^*(z)\right]\zeta_\alpha(z)\right]\\ &\quad+\frac{\hbar P}{2im_0}[\zeta_u(z)\zeta_v^*(z)-\zeta_u^*(z)\zeta_v(z)]\ .\end{aligned} \tag{2.12}$$

The last term of the right-hand side of the above equation arises due to the presence of off-diagonal elements in the effective-mass Hamiltonian (2.5) for the X valley. The flux conservation condition is now written in terms of the interface matrix as

$$\tilde{T}_{BA}^{+}\begin{bmatrix}i\sigma_y&0&0\\0&i\sigma_y&-\tau P_B\\0&\tau P_B&i\sigma_y\end{bmatrix}\tilde{T}_{BA}=\begin{bmatrix}i\sigma_y&0&0\\0&i\sigma_y&-\tau P_A\\0&\tau P_A&i\sigma_y\end{bmatrix}, \tag{2.13}$$

where σ_y is the y component of Pauli's spin matrix, $\tau=(\sigma_z+1)/2$, and P_A and P_B are the momentum matrix element P of semiconductor A and B, respectively.

III. EMPIRICAL TIGHT-BINDING MODEL

A. Method of calculation

The conduction band for $k_x=k_y=0$ with the Δ_1 symmetry is described by six atomic orbitals consisting of s, p_z (simply denoted by p in the following), and s^* of a cation and an anion in a unit cell.[41] The equation of motion is

$$H_{00}\mathbf{C}_0(n)+H_{01L}\mathbf{C}_1(n)+H_{01R}\mathbf{C}_1(n+1)=E\mathbf{C}_0(n)\ ,$$
$$H_{11}\mathbf{C}_1(n+1)+H_{10L}\mathbf{C}_0(n)+H_{10R}\mathbf{C}_0(n+1)=E\mathbf{C}_1(n+1)\ , \tag{3.1}$$

where $\mathbf{C}_j$ $(j=1,0)$ is a vector consisting of the three components C_{s_j}, C_{p_j}, and $C_{s_j^*}$. Note that cations and anions are denoted by subscript 1 and 0, respectively, in this paper, which follows the conventional notation[61] but is opposite to that used in the linear-chain tight-binding model considered in I. The 3×3 matrices appearing in the above are defined as

$$H_{00}=\begin{bmatrix} E_{s_0} & 0 & 0 \\ 0 & E_{p_0} & 0 \\ 0 & 0 & E_{s_0^*} \end{bmatrix},\qquad H_{11}=\begin{bmatrix} E_{s_1} & 0 & 0 \\ 0 & E_{p_1} & 0 \\ 0 & 0 & E_{s_1^*} \end{bmatrix}, \tag{3.2}$$

and

$$\begin{Bmatrix} H_{01R} \\ H_{10L} \end{Bmatrix} = \begin{array}{c} \\ s_0 \\ p_0 \\ s_0^* \end{array} \begin{array}{c} \begin{array}{ccc} s_1 & p_1 & s_1^* \end{array} \\ \begin{bmatrix} V_{s_0s_1}/2 & \pm V_{s_0p_1}/2 & V_{s_0s_1^*}/2 \\ \mp V_{s_1p_0}/2 & V_{p_0p_1}/2 & \mp V_{p_0s_1^*}/2 \\ V_{s_1s_0^*}/2 & \pm V_{p_1s_0^*}/2 & V_{s_0^*s_1^*}/2 \end{bmatrix} \end{array}, \tag{3.3}$$

where the upper sign is for H_{01R} and the lower for H_{01L}. Others can be obtained by

$$H_{10R}=\begin{bmatrix} 1 & 0 & 0 \\ 0 & -1 & 0 \\ 0 & 0 & 1 \end{bmatrix}(H_{01R})^t\begin{bmatrix} 1 & 0 & 0 \\ 0 & -1 & 0 \\ 0 & 0 & 1 \end{bmatrix}. \tag{3.4}$$

The same relation holds between H_{10L} and H_{01L}.

This can readily be solved by setting $\mathbf{C}_0(n)=\exp(ikz_n^0)\mathbf{C}_0$ and $\mathbf{C}_1(n)=\exp(ikz_n^1)\mathbf{C}_1$ with $z_n^0=(n-1)a/2$ and $z_n^1=(n-l-1/2)a/2$. We have

$$H(k)\mathbf{C}(k)=E\mathbf{C}(k) \tag{3.5}$$

with

$$\mathbf{C}(k)=\begin{bmatrix} \mathbf{C}_1 \\ \mathbf{C}_0 \end{bmatrix} \tag{3.6}$$

and

$$H(k)=\begin{bmatrix} H_{11} & H_{10R}e^{ika/4}+H_{10L}e^{-ika/4} \\ H_{01R}e^{ika/4}+H_{01L}e^{-ika/4} & H_{00} \end{bmatrix}. \tag{3.7}$$

Now, consider the interface consisting of material A occupying the left-hand side $(z<0)$ and B the right-hand side $(z>0)$. The interface is chosen at the position of the interfacial As atom z_l^0. The equation of motion at the interface is explicitly written as

$$H_{01L}^A\mathbf{C}_1^A(l)+H_{00}^{AB}\mathbf{C}_0^{AB}(l)+H_{01R}^B\mathbf{C}_1^B(l+1)=E\mathbf{C}_0^{AB}(l)\ , \tag{3.8}$$

where we have allowed the orbital energies of the interfacial As atom to be different from those in bulk. By extrapolating the bulk equations past the interface from the left and right side of the interface and then taking their average, we have

$$\tfrac{1}{2}[H_{01L}^A\mathbf{C}_1^A(l)+H_{01L}^B\mathbf{C}_1^B(l)]+\tfrac{1}{2}(H_{00}^A+H_{00}^B)\mathbf{C}_0^{AB}(l)+\tfrac{1}{2}[H_{01R}^A\mathbf{C}_1^A(l+1)+H_{01R}^B\mathbf{C}_1^B(l+1)]=E\mathbf{C}_0^{AB}(l)\ , \tag{3.9}$$

where

$$\mathbf{C}_0^A(l)=\mathbf{C}_0^B(l)=\mathbf{C}_0^{AB}(l)\ . \tag{3.10}$$

The boundary conditions consist of Eq. (3.10) and those obtained by subtracting Eq. (3.9) from Eq. (3.8). We choose a simple arithmetic average of A and B for the orbital energies of the interfacial As atom, i.e., $H_{00}^{AB}=(H_{00}^A+H_{00}^B)/2$. Then, the boundary conditions are given by

$$H^A_{01L}\mathbf{C}^A_1(l)-H^A_{01R}\mathbf{C}^A_1(l+1)$$
$$=H^B_{01L}\mathbf{C}^B_1(l)-H^B_{01R}\mathbf{C}^B_1(l+1)\ . \quad (3.11)$$

The interface matrix can be calculated by substituting

$$\mathbf{C}_1(n)=\sum_\alpha \exp(ik_\alpha z^1_n)[\mathbf{C}_1(k_\alpha)\zeta_\alpha(z^1_n)+\mathbf{C}'_1(k_\alpha)\nabla\zeta_\alpha(z^1_n)] \quad (3.12)$$

$$\mathbf{C}_1(n)=\sum_\alpha \exp(ik_\alpha z^1_n)[\mathbf{C}_1(k_\alpha)\zeta_\alpha(z^1_n)+\mathbf{C}'_1(k_\alpha)\nabla\zeta_\alpha(z^1_n)]$$

into Eqs. (3.10) and (3.11), where $\mathbf{C}'(k_\alpha)$ is the change of $\mathbf{C}(k)$ to the lowest order in $k-k_\alpha$. Expand $H(k)$ into the power series

$$H(k)=H(k_\alpha)+(k-k_\alpha)aH'(k_\alpha)$$
$$+(k-k_\alpha)^2a^2H''(k_\alpha)/2+\cdots\ . \quad (3.13)$$

Using Eq. (2.2) we can easily show that

$$\mathbf{C}'(k_\alpha)=-i\sum_{j\neq\alpha}\mathbf{C}_j(k_\alpha)\frac{(j|H'(k_\alpha)|\alpha)}{\varepsilon_j-\varepsilon_\alpha}\ . \quad (3.14)$$

Further, the effective mass becomes

$$\frac{m_0}{m_\alpha}=\frac{2m_0a^2}{\hbar^2}\left[\tfrac{1}{2}(\alpha|H''(k_\alpha)|\alpha)+\sum_{j\neq\alpha}\frac{|(j|H'(k_\alpha)|\alpha)|^2}{\varepsilon_j-\varepsilon_\alpha}\right], \quad (3.15)$$

and the momentum matrix element P becomes

$$P=-i\frac{2m_0a^2}{\hbar^2}(u|H'(2\pi/a)|v)\ . \quad (3.16)$$

In the case of X valleys (for u and v), the states u and v should also be excluded in the sum over j in the above equations, because mixings between u and v to the lowest order in $k-k_\alpha$ are taken into account by the matrix effective-mass equation (2.5). The resulting equations constitute six independent boundary conditions which determine six unknown quantities $(\zeta^B_\alpha,\nabla_B\zeta^B_\alpha)$ $(\alpha=\Gamma,u,v)$ for a given set of $(\zeta^A_\alpha,\nabla_A\zeta^A_\alpha)$. These equations are written in the form of Eq. (2.9) and therefore the resulting interface matrix has the form given by Eq. (2.11).

B. Results

In actual calculations of the interface matrix, we use the parameters similar to those proposed for GaAs and AlAs by Schulman and Chang[41] and assume an arithmetic average of GaAs and AlAs for those of $Al_xGa_{1-x}As$ (virtual crystal approximation). The parameters are listed in Table I, where small spin-orbit interactions are neglected for simplicity because they are unimportant in conduction bands. Calculated energy bands for GaAs and AlAs are given in Fig. 1. Table II shows the corresponding $\mathbf{k}\cdot\mathbf{p}$ parameters of GaAs and AlAs calculated in the tight-binding model.

We immediately notice some limitations of the effective-mass approximation for the X valley. The 2×2 effective-mass equation predicts that the minima of the X valley in GaAs, for example, are at $\pm k_0$ with $k_0=0.154(2\pi/a)$ away from the X point, while the exact diagonalization of Eq. (3.7) gives $k_0=0.123(2\pi/a)$. Such deviations from the effective-mass approximation are not surprising because the effective mass at the X point is very large and the distance of minimum from the X point already exceeds 10% of that between the Γ and X point. We may have to redefine parameters such as m_u, m_v, E_u, E_v, and P so as to reproduce overall features of the dispersion instead of using the parameters given directly from the $\mathbf{k}\cdot\mathbf{p}$ perturbation. This does not have so much meaning, however, because the present understanding of the band structure in the vicinity of the X point is insufficient to determine these parameters and because the accuracy of the result of the tight-binding model itself is also uncertain.

Examples of calculated $\tilde{T}_{BA}$'s for GaAs/$Al_xGa_{1-x}As$ with $x=0.3$ and 0.6 are given in Table III. First, we notice that all the off-diagonal elements except $t^{\Gamma v}_{21}$ and $t^{v\Gamma}_{21}$ are very small and that the diagonal elements are close to unity. This suggests that mixings of Γ and X valleys at the interface can be approximately described by the interface matrix whose diagonal elements are all unity and whose off-diagonal elements are neglected except $t^{\Gamma v}_{21}$, $t^{v\Gamma}_{21}$, t^{uv}_{21}, and t^{vu}_{21}. The latter two elements are required only because of the flux conservation in the X valleys, i.e., $t^{uv}_{21}\lesssim(P_B-P_A)/2$ and $t^{vu}_{21}\lesssim-(P_B-P_A)/2$. Calculations for interfaces of $Al_xGa_{1-x}As$ with different x's reveal that both $t^{\Gamma v}_{21}$ and $t^{v\Gamma}_{21}$ are approximately proportional to the difference in the Al contents of the two materials, i.e.,

TABLE I. Tight-binding parameters for GaAs and AlAs used in the present calculation. Spin-orbit interactions are neglected.

Parameters	GaAs (eV)	AlAs (eV)
E_{s_0}	−8.4570	−7.6201
E_{s_1}	−2.7788	−1.1786
E_{p_0}	0.9275	0.8905
E_{p_1}	3.5547	3.4939
$E_{s^*_0}$	8.4775	7.3905
$E_{s^*_1}$	6.6247	6.6339
$V_{s_0s_1}$	−6.4513	−6.6642
$V_{s_0p_1}$	4.4800	5.1106
$V_{s_0s^*_1}$	0.0000	0.0000
$V_{s_1p_0}$	7.8500	6.3000
$V_{s_1s^*_0}$	0.0000	0.0000
$V_{p_0p_1}$	1.9546	1.8780
$V_{p_0s^*_1}$	7.0500	7.2000
$V_{p_1s^*_0}$	4.7922	4.5216
$V_{s^*_0s^*_1}$	0.0000	0.0000

TABLE II. Effective-mass parameters for the Γ and X valleys calculated in the tight-binding model. The energy origin is at the top of the valence band. The wave vector k_0 and the energy E_X are calculated using the matrix effective-mass equation for the X valley, and the numbers in parentheses for k_0 and E_X represent those calculated directly in the tight-binding model.

Parameters	GaAs	$Al_{0.3}Ga_{0.7}As$	$Al_{0.6}Ga_{0.4}As$	AlAs
E_Γ (eV)	1.544	2.009	2.474	3.095
E_u (eV)	2.073	2.143	2.213	2.300
E_v (eV)	2.293	2.223	2.167	2.119
P	1.588	1.897	2.224	2.688
m_Γ (m_0)	0.0679	0.100	0.142	0.222
m_u (m_0)	1.350	1.410	1.477	1.580
m_v (m_0)	1.575	1.409	1.270	1.117
k_0 ($2\pi/a$)	0.154	0.211	0.241	0.275
	(0.123)	(0.169)	(0.190)	(0.209)
E_X (eV)	2.049	2.030	1.989	1.926
	(2.056)	(2.051)	(2.021)	(1.973)

$t_{21}^{\Gamma v} \approx -p(x_B - x_A)$ and $t_{21}^{v\Gamma} \approx q(x_B - x_A)$, where both p and q are a quantity of the order of unity.

Unfortunately, the resulting 6×6 interface matrix does not satisfy the flux conservation condition Eq. (2.13) exactly. Table IV compares the left-hand side of Eq. (2.13) with the right-hand side for $x=0.3$. We see that the left-hand side of Eq. (2.13) gives rise to off-diagonal elements with respect to Γ and v. This slight violation of the flux conservation is presumably inherent to the present approximation scheme in connecting envelopes of Γ and X valleys. Note that the flux conservation is satisfied quite well within each valley, however.

We have assumed that waves associated with the Γ and X minima possess energy equal to each other. In Eq. (2.1) those waves are all expressed in terms of the solutions calculated by the $\mathbf{k}\cdot\mathbf{p}$ perturbation around each extremum point. The $\mathbf{k}\cdot\mathbf{p}$ solution is exact only to the lowest order in $(k-k_\alpha)a$,[59] and, therefore, the energy of the waves can actually be slightly different from each other. The linear combination of waves with different energies gives rise to a flux oscillating in time[62] and the condition (2.13) need not be satisfied. For practical purposes this slight violation of the conservation law does not give rise to any serious problems as long as we keep this fact in mind in actual calculations.

When the energy at the X minima is sufficiently high in comparison with that of the Γ minima, we can eliminate the presence of the X valleys regarding them as evanescent waves and express the boundary conditions for the Γ valley envelopes by a 2×2 interface matrix. There are two ways to determine this 2×2 matrix. The first is to introduce two exact evanescent waves at the energy of the Γ minimum in each material and then solve the equation giving the boundary conditions ($\tilde{T}_{BA}^{(1)}$). We can also calculate it from the above 6×6 matrix by replacing the X-valley envelopes by evanescent solutions of the effective-mass equation ($\tilde{T}_{BA}^{(2)}$). The consistency requires, of course, that these two methods should give results very close to each other.

For $GaAs/Al_xGa_{1-x}As$ ($x=0.3$), we have explicitly

TABLE III. Examples of 6×6 interface matrices for $GaAs/Al_xGa_{1-x}As$ interface with $x=0.3$ and 0.6.

$x=0.3$	ζ_Γ^A	$\nabla_\Gamma^A\zeta_\Gamma^A$	ζ_u^A	$\nabla_u^A\zeta_u^A$	ζ_v^A	$\nabla_v^A\zeta_v^A$
ζ_Γ^B	1.063	0.000	−0.015	0.000	0.000	−0.005
$\nabla_\Gamma^B\zeta_\Gamma^B$	0.000	0.953	0.000	0.020	−0.360	0.000
ζ_u^B	0.003	0.000	0.974	0.000	0.000	−0.003
$\nabla_u^B\zeta_u^B$	0.000	−0.005	0.000	0.992	0.061	0.000
ζ_v^B	0.000	0.006	0.000	−0.011	0.950	0.000
$\nabla_v^B\zeta_v^B$	0.244	0.000	−0.099	0.000	0.000	1.059
$x=0.6$	ζ_Γ^A	$\nabla_\Gamma^A\zeta_\Gamma^A$	ζ_u^A	$\nabla_u^A\zeta_u^A$	ζ_v^A	$\nabla_v^A\zeta_v^A$
ζ_Γ^B	1.132	0.000	−0.031	0.000	0.000	−0.011
$\nabla_\Gamma^B\zeta_\Gamma^B$	0.000	0.896	0.000	0.048	−0.686	0.000
ζ_u^B	0.004	0.000	0.948	0.000	0.000	−0.007
$\nabla_u^B\zeta_u^B$	0.000	−0.007	0.000	0.981	0.125	0.000
ζ_v^B	0.000	0.013	0.000	−0.020	0.894	0.000
$\nabla_v^B\zeta_v^B$	0.554	0.000	−0.203	0.000	0.000	1.118

TABLE IV. Comparison of the left- (without parentheses) and right- (in parentheses) hand sides of Eq. (2.13) for GaAs/$Al_xGa_{1-x}As$ ($x=0.3$).

(2.13)	ξ_Γ^B	$\nabla_\Gamma^B\xi_\Gamma^B$	ξ_u^B	$\nabla_u^B\xi_u^B$	ξ_v^B	$\nabla_v^B\xi_v^B$
ξ_Γ^B	0.000	1.011	0.000	0.027	0.619	0.000
	(0)	(1)	(0)	(0)	(0)	(0)
$\nabla_\Gamma^B\xi_\Gamma^B$	−1.011	0.000	0.030	0.000	0.000	0.011
	(−1)	(0)	(0)	(0)	(0)	(0)
ξ_u^B	0.000	−0.030	0.000	0.984	−1.595	0.000
	(0)	(0)	(0)	(1)	(−1.588)	(0)
$\nabla_u^B\xi_u^B$	−0.027	0.000	−0.984	0.000	0.000	−0.008
	(0)	(0)	(−1)	(0)	(0)	(0)
ξ_v^B	−0.619	0.000	1.595	0.000	0.000	0.999
	(0)	(0)	(1.588)	(0)	(0)	(1)
$\nabla_v^B\xi_v^B$	0.000	−0.011	0.000	0.008	−0.999	0.000
	(0)	(0)	(0)	(0)	(−1)	(0)

$$\tilde{T}_{BA}^{(1)}=\begin{bmatrix}1.054 & -0.000\\ -0.027 & 0.949\end{bmatrix}$$

and (3.17)

$$\tilde{T}_{BA}^{(2)}=\begin{bmatrix}1.064 & -0.000\\ 0.037 & 0.953\end{bmatrix}.$$

These two give negligibly small off-diagonal elements t_{21} and t_{12} and diagonal elements which agree with each other within 1%. Note that $\tilde{T}_{BA}^{(2)}$ slightly violates flux conservation in contrast to $\tilde{T}_{BA}^{(1)}$, which is closely related to the violation existing in the original 6×6 interface matrix. We can normalize $\tilde{T}_{BA}^{(2)}$ so as to fulfill the conservation condition in such a way that its determinant is unity. We get $t_{11}=1.056$ and $t_{22}=0.947$ which are much closer to $\tilde{T}_{BA}^{(1)}$.

It should be noticed that $\tilde{T}_{BA}^{(2)}$ is very close to $\tilde{T}_{BA}^{\Gamma\Gamma}$ given in Table III. This shows that the boundary conditions for the Γ-valley envelopes are little affected by the presence of the X valleys. The same is applicable to a 4×4 interface matrix describing connection of envelopes associated with the X valleys when the Γ-valley energy is sufficiently far. Small mixings can be included by the elements $t_{21}^{\Gamma v}$ and $t_{21}^{v\Gamma}$ which are approximately proportional to the difference in the Al content of two alloys. The coefficients p and q may depend on the model used for calculation but are expected to be a constant of the order of unity irrespective of models.

IV. APPLICATIONS

The 6×6 interface matrix calculated in the previous section can be used to study various problems. In this section, demonstrations will be made within a simplified model of the interface matrix and the band structure in the vicinity of the X points. First, we assume for simplicity that $m_u=m_v=0.85m_0$ and $P=2.0$ independent of x because of the lack of detailed experimental information on the dispersion in the vicinity of the X points. We assume further $m_\Gamma\approx(0.067+0.057x)m_0$, $E_\Gamma(x)\approx 1.0x$ (eV), $E_u\approx 0.6-0.4x$ (eV), and $E_v\approx 0.8-0.4x$ (eV). This leads to $m_X\approx 1.12m_0$ independent of x and $E_X\approx E_u-0.026$ (eV). Mendez *et al.* assumed $m_X=0.85m_0$ in analyzing their experiments on tunnelings via X-valley states.[23–25] More recent experiments of photoluminescence[22] suggested a heavier mass $m_X\sim 1.2m_0$ Note that we have assumed that E_u and E_v do not cross with increasing x contrary to the result of the tight-binding model. As for the 6×6 interface matrix, all the diagonal elements are replaced by unity (the envelope-function approximation) and mixings between different valleys are described by the off-diagonal elements $t_{21}^{v\Gamma}$ and $t_{21}^{\Gamma v}$ only. For simplicity, we assume $p\approx q\approx 1$. The off-diagonal elements t_{21}^{uv} and t_{21}^{vu} need not be included because we have

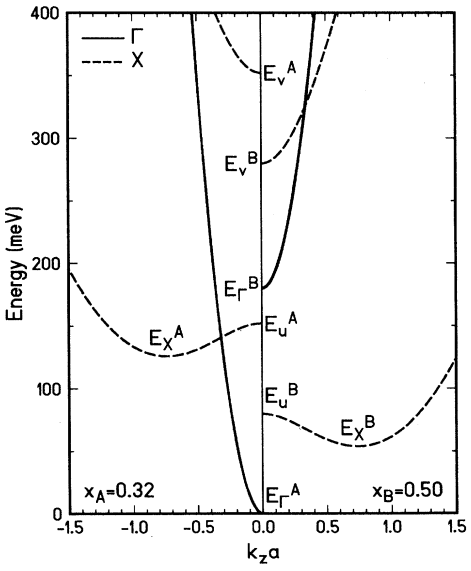

FIG. 2. The energy dispersion of the Γ (solid lines) and X valleys (dashed lines) for a model system. The wave vector is measured from the extremum point of each valley. The left panel shows that of $Al_xGa_{1-x}As$ with $x=0.32$ (A) and the right with $x=0.5$ (B).

assumed that P is independent of x.

In the following, we shall exclusively consider the interface of $Al_xGa_{1-x}As$'s with $x=0.32$ and 0.5. This combination is chosen because the relative position of the Γ and X valleys is intriguing. As is shown in Fig. 2, the bottom of the X valleys for $x=0.5$ is below that for $x=0.32$ but still higher than the bottom of the Γ valley for $x=0.32$. Therefore, if we make a barrier of $Al_xGa_{1-x}As$ layer with $x=0.5$ by sandwiching it by $Al_xGa_{1-x}As$ layers with $x=0.32$, there can be virtual bound states associated with the X valleys in the barrier layer.

A. Transmission and reflection at heterointerfaces

Let us first consider reflections and transmissions of electron waves at a single interface consisting of $Al_xGa_{1-x}As$ with $x_A=0.32$ (left-hand side) and $x_B=0.5$ (right-hand side). An electron in the Γ valley is incident from the left-hand side. Calculated transmission and reflection coefficients are given in Fig. 3. With increasing energy, the transmission into the X valley starts to take place when the energy E reaches E_X^B, the bottom of the X valley of B, reaches a maximum when $E=E_u^B$, and reaches another maximum when the energy is at the bottom of the X valley of A, i.e., $E=E_X^A$. With further increase, the transmission decreases due to opening of the channel of reflection into the X valley of the left material. There appears a small structure at $E=E_u^A$, and finally, when the energy is beyond the bottom of the Γ valley or the right-hand side, the transmission increases drastically and rapidly approaches unity. The maximum transmission from the Γ to X valleys is about 1%. There exists an energy between E_u^B and E_X^A where the transmission nearly vanishes. This is presumably due to formation of an interface resonance state using evanescent waves arising from states near E_X^A and E_u^B. The reflection into the Γ valley remains almost unity up to $E=E_\Gamma^B$ in spite of the presence of small transmission probabilities into the X valleys.

Figure 4 shows the transmission probability for a single-barrier structure consisting of $Al_xGa_{1-x}As$. The barrier layer has $x=0.5$ and is sandwiched by layers with $x=0.32$. When the thickness of the barrier is small (50 Å), the tunneling is dominated by the Γ-Γ channel. At energies of virtual bound levels associated with the X valleys, the transmission exhibits resonances and antiresonances due to constructive and destructive interferences of electron waves in the Γ and X valleys. Except for the presence of narrow peaks and dips, the tunneling probability is very close to that calculated in the envelope-function approximation, i.e., by neglecting mixings between different valleys at the interface.

When the thickness of the barrier layer becomes larger and the tunneling probability calculated in the EFA is reduced, the tunneling is dominated by the Γ-X-Γ channel in the whole energy range shown in the figure. There are many virtual bound states because of the large effective mass of the X valley. After averaging out narrow peaks and dips due to such virtual bound states, the remaining tunneling probability exhibits a maximum around $E\approx E_u^B$ and takes a minimum at an energy between E_u^B and E_X^A. This reflects the energy dependence of the transmission coefficient at the single interface shown in the previous figure. When the energy exceeds E_X^A, there appears a

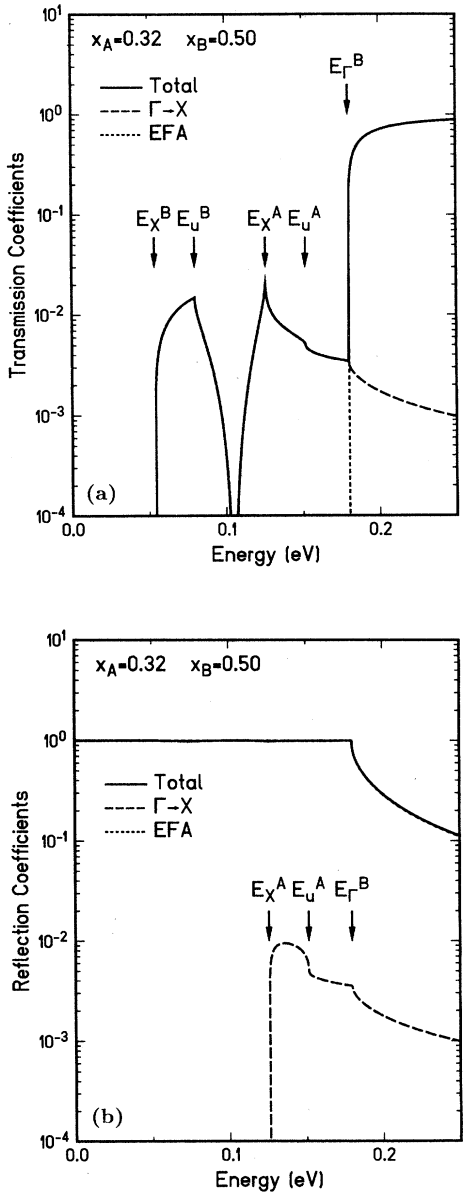

FIG. 3. (a) Calculated transmission coefficients and (b) reflection coefficients at an $Al_xGa_{1-x}As$ single interface. Electron waves in the Γ valley are incident on the interface consisting of an alloy with $x=0.32$ occupying the left-hand side (A) and that with $x=0.5$ occupying the right-hand side (B). The dotted line represents the results calculated by neglecting mixings of different valleys, i.e., in the EFA, the dashed lines are transmissions or reflections into the X valley, and the solid lines are the total. Maximum transmissions and reflections into the valleys are about 1%.

strong tunneling into the X valleys due to the opening of the Γ-X channel.

In the above calculations, the violation of the flux conservation existing in T_{BA} can give rise to results which do not satisfy the condition $T+R=1$, with T and R the total transmission and reflection probability, respectively. Actually, the results shown in Figs. 3 and 4 have been renormalized so as to satisfy $T+R=1$. The deviation of $T+R$ from unity is usually very small. The only exceptions are at energies of virtual bound states associated with the X valley in Fig. 4, where the deviation can be appreciable (sometimes as large as a few tens of percent).

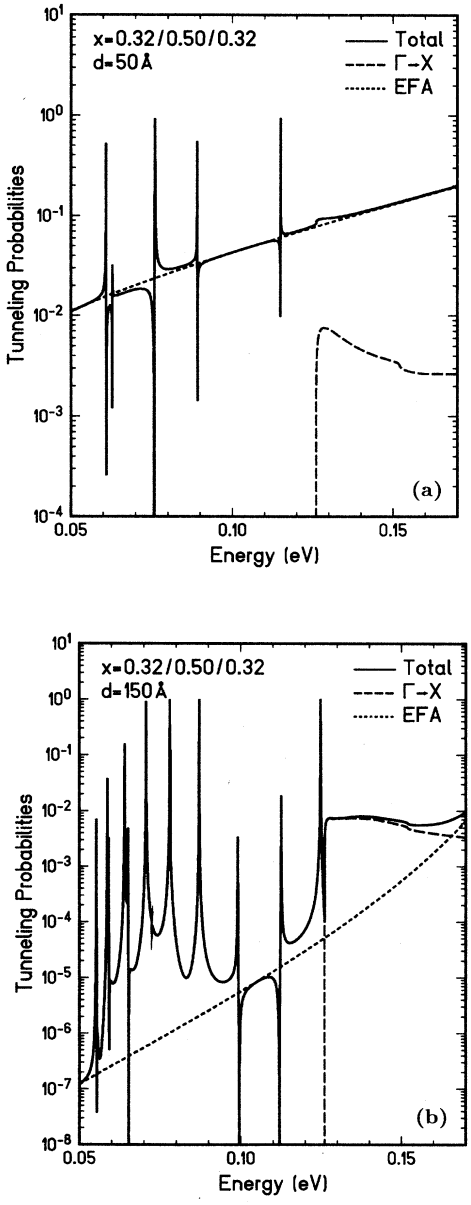

FIG. 4. Calculated tunneling probabilities as a function of energy across a single-barrier structure consisting of $Al_{0.32}Ga_{0.68}As$, $Al_{0.5}Ga_{0.5}As$, and $Al_{0.32}Ga_{0.68}As$. Electrons are incident from the left-hand side in the Γ valley. When the barrier thickness d is small [(a) $d=50$ Å] and the tunneling within the Γ valley is dominant, the presence of virtual bound states in the X valley in the barrier layer gives rise to small constructive and destructive interferences with waves in the Γ valley. With the increase of the barrier thickness [(b) $d=150$ Å], the tunneling through Γ-X-Γ channels becomes dominant.

Sharp peaks and spikes appearing at energies of X-valley virtual bound states are qualitatively similar to those obtained by calculations in tight-binding and pseudopotential models.[50,53–55] The sharp structures are easily smeared out and may not be observed in tunneling experiments, because the tunneling current is the sum of contributions for states with different energies. Mendez *et al.* measured tunneling probabilities in double-barrier structures under high pressures.[25] They have observed a sudden increase of tunneling currents under a constant bias when the applied pressure exceeds a certain critical value. Similar phenomena have been observed also by Solomon *et al.*[28] This decrease of the effective barrier height is qualitatively explained by the increase of tunneling via X-valley states caused by the lowering of the X-valley bottom under high pressures.

Unfortunately, more detailed comparison with tunneling experiments is not feasible because the band parameters in the vicinity of the X point have not been accurately known. However, our formalism can easily be applied to calculations of tunneling currents under experimental conditions once various band parameters are known. In order to calculate tunneling currents as a function of a bias voltage across the barrier, we have to integrate the tunneling probability over energy up to the Fermi level in incident electrons. In electric fields, we can expect much richer structures in the energy dependence of the tunneling probabilities due to the presence of various virtual bound states.[23–25,55] After integration over energy, however, most of small peaks and dips are likely to be smeared out. Note, further, that the presence of other X valleys should be considered when the barrier layer consists of alloy $Al_xGa_{1-x}As$. Due to alloy disorder in the barrier layer, electrons can be scattered from the Γ valley to transverse X valleys located in the direction parallel to the interface. It has been shown that this process can modify tunneling probabilities drastically.[63]

B. Energy levels in a superlattice

The 6×6 interface matrix can also be used in calculating mixing effects on energy levels and wave functions in $GaAs/Al_xGa_{1-x}As$ superlattices. Explicit calculations can be performed variationally by expanding the wave function in terms of an orthonormal basis set and by treating the boundary conditions as terms in the Hamiltonian matrix. This is quite similar to the method described in more detail for calculations of phonon spectra.[64]

Figure 5 gives the energy dispersion in an $Al_xGa_{1-x}As$ superlattice consisting of a layer with the Al content $x_A=0.32$ and the thickness $d_A=52$ Å and that with $x_B=0.5$ and $d_B=48$ Å. Only the lowest subband shown

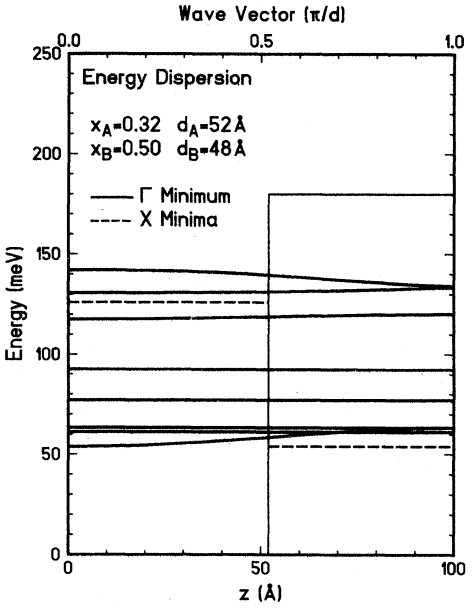

FIG. 5. Calculated subband dispersion in a superlattice consisting of $Al_xGa_{1-x}As$ with $x_A=0.32$ and $x_B=0.5$. The thickness of the layer A (left-hand side) is $d_A=52$ Å and that of B (right-hand side) is $d_B=48$ Å. The bottom of the X valley is shown by the horizontal dashed lines. At $k_z=0$, only the lowest subband has Γ-valley characters and the others all have X-valley characters. For large k_z these subbands associated with different valleys cross in energy, where a very small energy splitting appears due to mixing effects.

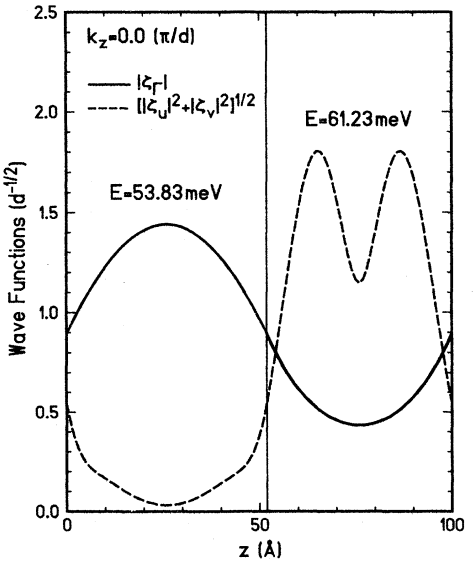

FIG. 6. Calculated envelope functions for the lowest two subbands at $k_z=0$ for an $Al_xGa_{1-x}As$ superlattice. The parameters are the same as in Fig. 5. Mixings between different valleys are negligibly small for both subbands.

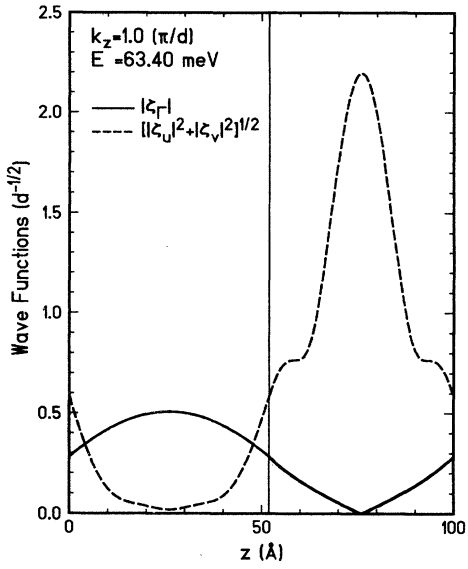

FIG. 7. Calculated envelope functions for the first excited subband at $k_z=\pi/d$ for the $Al_xGa_{1-x}As$ superlattice. The parameters are the same as in Fig. 5. Envelopes are strongly mixed with each other.

in the figure is associated with the Γ valley and all other subbands have essentially a character of the X valley. Figure 6 gives examples of calculated wave functions of the lowest two subbands at $k_z=0$. The Γ-like lowest subband has an appreciable amplitude in the barrier layer. On the other hand, the wave function of the X-like first excited subband is strongly localized in the barrier layer and exhibits an oscillation due to the double-minima structure of the conduction band in the vicinity of the X point. Couplings of energy levels and wave functions of the Γ and X valleys are small and negligible as long as their energy levels are sufficiently far from each other. Mixings become appreciable only when their energies are close to each other as shown in Fig. 7, which gives envelope functions of the first excited subband at $k_z=\pi/d$ with $d=d_A+d_B$. The splitting of energies of the first and second excited subbands remains less than 1 meV at $k_z=\pi/d$.

V. TUNNELING ACROSS HIGH BARRIER

The interface matrix can be extended so as to treat problems of tunneling across high barriers, to which the conventional envelope-function approximation is not directly applicable. Consider a barrier with width d. The interface matrix now relates the envelope at the left side of the barrier ($z=0$) and that at the right side of barrier ($z=d$), i.e.,

$$\begin{bmatrix} \zeta(d) \\ \nabla\zeta(d) \end{bmatrix} = T(d) \begin{bmatrix} \zeta(0) \\ \nabla\zeta(0) \end{bmatrix}, \tag{5.1}$$

where $T(d)=(t_{ij})$ is a 2×2 matrix. In this section, we shall confine ourselves to the case of a single conduction-

band minimum.

It is straightforward to calculate transmission and reflection coefficients across the barrier once $T(d)$ is given. One way to characterize properties of barriers is to use the scattering matrix S, defined by

$$S=\begin{matrix} \\ o \\ o' \end{matrix}\begin{matrix} \begin{matrix} i & i' \end{matrix} \\ \begin{bmatrix} r & t' \\ t & r' \end{bmatrix} \end{matrix}, \tag{5.2}$$

where i and o denote incoming and outgoing channels, respectively, in the left-hand side of the barrier, and i' and o' are corresponding channels in the right-hand side. The flux conservation leads to the unitarity of the S matrix, i.e., $S^{+}S=1$, and the time reversal symmetry leads to $t=t'$.

When the incident energy is sufficiently small, we can expand the S matrix in terms of k_A and k_B and have

$$\begin{aligned} t=t'&=-i(k_A k_B)^{1/2}\eta[1+i(k_A+k_B)\delta+\cdots], \\ r&=(1-|t|^2)^{1/2}\exp(2ik_A\delta), \\ r'&=(1-|t|^2)^{1/2}\exp(2ik_B\delta), \end{aligned} \tag{5.3}$$

where k_A and k_B are the wave vector in the material A occupying the left-hand side of the barrier ($z<0$) and that in B occupying the right-hand side ($z>d$), respectively. In the above, we have introduced η and δ, both of which have the dimension of length. They are expressed in terms of elements of $T(d)$ as

$$\eta=2a/t_{21} \quad \text{and} \quad \delta=at_{11}/t_{21}. \tag{5.4}$$

The former parameter η is proportional to the transmission coefficient and therefore will be called "tunneling length." The latter parameter δ describes the penetration depth into the barrier. The meaning of δ becomes clear if we consider a series of two barriers characterized by the S matrix S_1 and S_2. The total S matrix becomes

$$t=\frac{t_1\tilde{t}_2}{1-r_1'\tilde{r}_2}, \quad r=r_1+\frac{\tilde{r}_2 t_1^2}{1-r_1'\tilde{r}_2}, \quad r'=r_2'+\frac{r_1'\tilde{t}_2^2}{1-r_1'\tilde{r}_2}, \tag{5.5}$$

with $\tilde{r}_2=r_2\exp(2ikL)$ and $\tilde{t}_2=t_2\exp(ikL)$, where k is the wave vector in the layer sandwiched by the barrier 1 and 2 and L is its thickness. The resonant tunneling occurs under the condition $k(L+\delta_1+\delta_2)=2\pi j$ with integer j in the limit of small $|t|$ and $|t'|$, demonstrating the increase of the well width by the penetration depth.

In the following, we consider GaAs/$Al_xGa_{1-x}As$/GaAs(001) barrier structures with different x. In this case, we have the relation

$$T(d)=\sigma_z T(d)^{-1}\sigma_z, \tag{5.6}$$

which is obtained from a symmetry relation under a mirror reflection around the center of the barrier layer similar to Eq. (2.12) of I and by noting the fact the system is invariant under the reflection. This gives the condition that $t_{11}=t_{22}$. Since we have the condition of flux conservation $\det T(d)=1$, there exist only two independent parameters. The expression of the S matrix is also characterized by the two quantities η and δ.

It is almost straightforward to calculate the interface matrix $T(d)$ if we use the *sps** tight-binding model employed in the previous sections. At $z=0$ the amplitudes

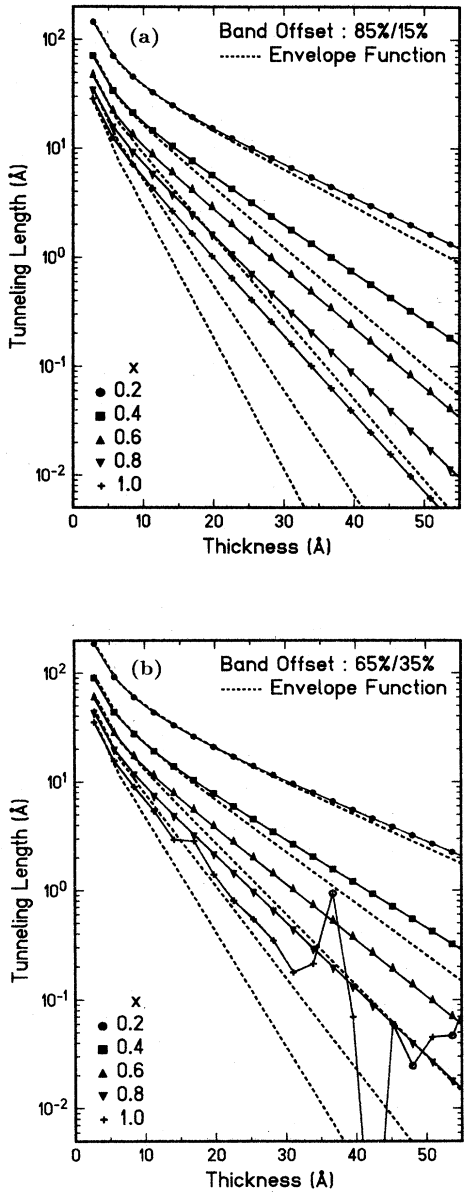

FIG. 8. Calculated tunneling length η (proportional to the tunneling probability) as a function of the thickness of the barrier $Al_xGa_{1-x}As$ layer for different x's. (a) 85%:15% rule and (b) 65%:35% rule. For high potential barriers the envelope-function approximation underestimates the tunneling probability considerably. For $x=1$ in (b), the tunneling length exhibits nonsmooth dependence on the barrier thickness and can also be negative (open circles) due to resonances and antiresonances with virtual bound states associated with the X valley.

$\mathbf{C}(z=0)$ of atomic orbitals are expressed in terms of a linear combination of the envelope associated with the Γ-valley conduction-band minimum of the left-hand material, its first derivative, and amplitudes of two evanescent waves associated with the X valleys. The amplitudes $\mathbf{C}(z=d)$ of atomic orbitals at $z=d$ are obtained directly by multiplying tight-binding matrices iteratively starting from $\mathbf{C}(0)$. On the other hand, the amplitudes $\mathbf{C}(d)$ can similarly be expressed in terms of the envelope and amplitudes of evanescent waves of the right-hand material. The results constitute a set of six equations which determine $\zeta(d)$ and $\nabla\zeta(d)$ together with amplitudes of four evanescent waves for a given set of $\zeta(0)$ and $\nabla\zeta(0)$.

Figure 8 gives examples of calculated tunneling lengths as a function of the barrier thickness for different x's. The two kinds of band-offset parameters are assumed, i.e., Dingle's 85%:15% rule[65] and more recent 65%:35% rule.[66] With increasing barrier thickness, the tunneling probability decreases exponentially except in the case of $x=1$ for the 65%:35% rule. Figure 9 shows energies of the Γ and X conduction-band minima of $Al_xGa_{1-x}As$ measured from the Γ minimum of GaAs at GaAs/$Al_xGa_{1-x}As$ interfaces. As can be seen, the X bottom of AlAs becomes lower than the Γ minimum of GaAs in the present tight-binding model if the 65%:35% rule is used. This gives rise to the nonsmooth dependence on the thickness due to interferences with virtual bound states associated with the X valleys in the barrier $Al_xGa_{1-x}As$ layer.

When the barrier height is small, i.e., for small x, the tunneling probability is very close to that calculated in the EFA. With the increase of the barrier height, however, the EFA tends to underestimate the tunneling probability. Figure 10 gives the penetration depth divided by δ_0 which is the penetration depth calculated in the EFA for infinitely thick barriers. We have explicitly $\delta_0=(m'/m)(\hbar^2/2m'V)^{1/2}$ with m and m' the effective mass of GaAs and $Al_xGa_{1-x}As$, respectively, and V the barrier height. The effective penetration becomes smaller than that calculated in the EFA. This is quite in contrast to the behavior of the tunneling probability. We would expect that the smaller penetration into the barrier leads to small tunneling probability.

In order to determine whether mixings between Γ and

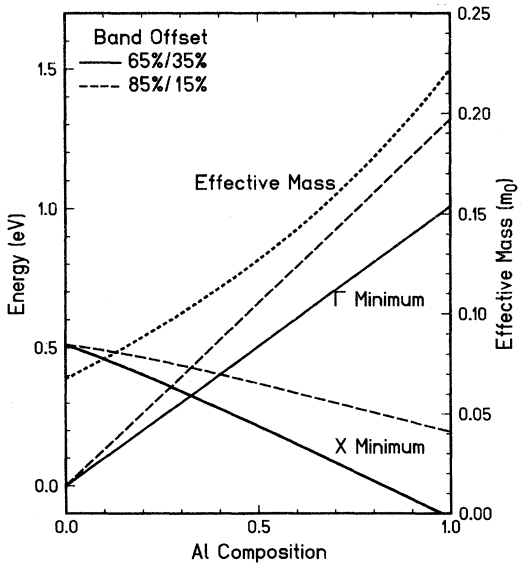

FIG. 9. Energies of various conduction-band minima of $Al_xGa_{1-x}As$ at GaAs/$Al_xGa_{1-x}As$ heterointerfaces calculated in the *sps** tight-binding model as a function of the Al content x measured from the bottom of the Γ minimum of GaAs. The effective mass at the Γ valley is also included (dotted line).

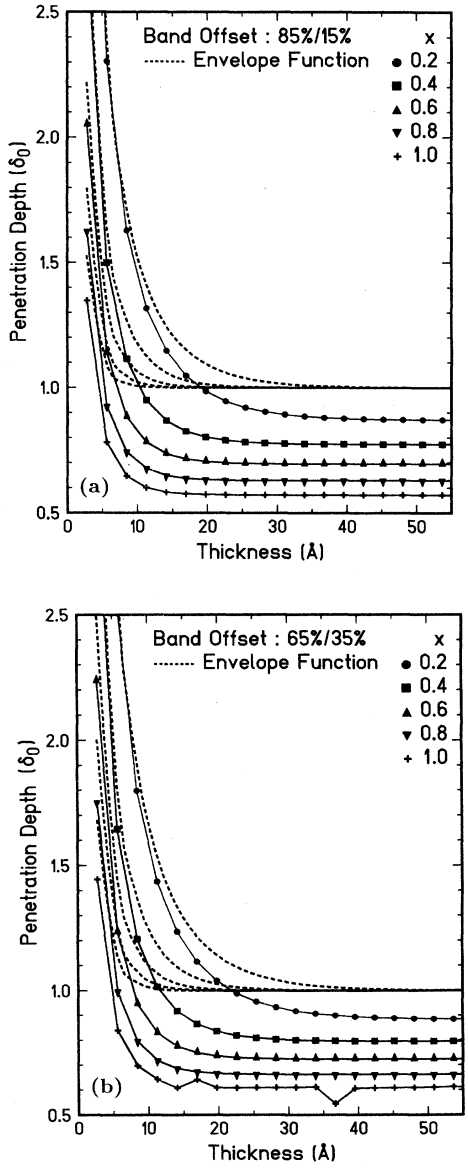

FIG. 10. Calculated penetration depth δ as a function of the thickness of the barrier $Al_xGa_{1-x}As$ layer for different x's. (a) 85%:15% rule and (b) 65%:35% rule. The penetration depth is normalized by the corresponding quantity δ_0 calculated in the envelope-function approximation for infinitely thick barriers.

X are responsible for this controversy, we can use the 6×6 interface matrix calculated in the previous section. The results of such calculations show that the penetration depth becomes smaller due to deviation of diagonal elements t_{11}^{Γ} and t_{22}^{Γ} from unity (see Table III, for example). However, the tunneling probability becomes slightly smaller than that calculated in the EFA except in the case that the X minimum in the barrier layer is lower than the incident electron energy. The major origin of the discrepancy of the tunneling probability is the nonparabolicity of the conduction band.

Figure 11 gives the effective mass as a function of energy measured from the valence-band top of $Al_xGa_{1-x}As$ in the band-gap region. The effective mass is defined by $(1/2\hbar^2)(\partial k^2/\partial E)$ with k the (imaginary) wave vector of waves associated with the Γ conduction-band minimum or valence-band top at energy E. It shows that the mass in the band gap becomes considerably smaller than the band-edge mass with decreasing energy. This means that the decay length of the evanescent waves associated with the Γ conduction-band minimum can be much larger than that calculated in the EFA, leading to larger tunneling probability. This seems to agree with the conclusion obtained by Ko and Inkson,[55] who used an empirical pseudopotential model. Reliable estimates of tunneling probabilities may be made even in the EFA if we use a $\mathbf{k}\cdot\mathbf{p}$ Hamiltonian containing both the conduction band and the valence bands.[67] Tsuchiya and Sakaki have measured escape rates of an electron from a GaAs quantum well across AlAs barriers with different thicknesses and shown that they are explained reasonably well by calculations in the effective-mass approximation.[68] In their analysis, they have assumed that the effective mass in the barrier layer is the same as that of the conduction-band bottom of GaAs.

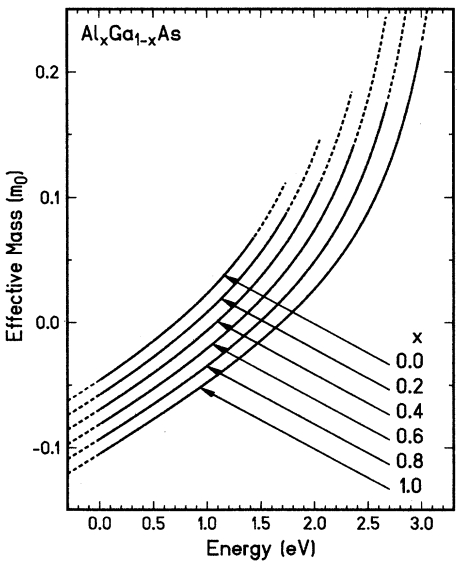

FIG. 11. Effective masses of $Al_xGa_{1-x}As$ calculated in the *sps** tight-binding model as a function of energy measured from the valence-band top. The solid lines represent those in the band gap and the dashed lines in the conduction and valence bands.

VI. SUMMARY AND CONCLUSION

We have presented a formalism in which mixings of the Γ and X valleys at $GaAs/Al_xGa_{1-x}As$ heterointerfaces are treated within the effective-mass approximation. Effects of the presence of interfaces are included in boundary conditions for envelope functions and their derivatives at interfaces expressed in terms of a 6×6 interface matrix. The interface matrix has been calculated in an *sps** tight-binding model with nearest-neighbor transfer integrals.

The calculated interface matrix slightly violates the flux conservation across the interface due to the difference in energies of the Γ and X conduction-band minima in bulk. Mixings at the interface are described by two off-diagonal elements which are roughly proportional to the difference in the Al content x of the two materials. The proportionality coefficients have turned out to be almost unity in the tight-binding model. Actual numbers may strongly depend on models used for calculations and should rather be regarded as parameters to be determined experimentally.

As a demonstration, transmission and reflection coefficients across a single interface have been calculated. The results exhibit interesting features due to the Γ-X mixings. Same calculations have been made for a single-barrier structure. The presence of virtual bound states associated with the X valleys in the barrier layer gives rise to constructive and destructive interferences in the tunneling probability for electron incident in the Γ valley. Except for the presence of sharp peaks and dips due to such interferences, the Γ-X mixings are not important for small barrier widths. Only when the barrier becomes thicker and the tunneling probability calculated in the conventional envelope-function approximation becomes extremely small, tunnelings via X-valley states become dominant. The 6×6 interface matrix has been used also in calculating energy levels and wave functions in a multiple-quantum-well structure. Mixing effects have turned out to be very small again except in the case where energy levels associated with the Γ and X valleys cross with each other.

The interface matrix is also useful in studying a tunneling problem across high potential barriers to which the envelope-function approximation is not applicable. The 2×2 interface matrix of Γ-valley electrons for $GaAs/Al_xGa_{1-x}As/GaAs$ barrier structures has been calculated in the *sps** tight-binding model. It has been shown again that mixings between the Γ and X valleys are usually unimportant. The nonparabolicity of effective masses within the band gap of barrier materials plays a more important role in enhancing tunneling probabilities than that calculated in the envelope-function approximation.

ACKNOWLEDGMENTS

This work is supported in part by Grant-in-Aid for Specially Promoted Research from the Ministry of Education, Science and Culture, Japan.

[1]See, for example, M. Altarelli, in *Third Brazilian School of Semiconductor Physics,* edited by C. E. T. Gonçalves da Silva and L. E. Oliveira (World Scientific, Singapore, 1987), p. 3.
[2]T. Ando, S. Wakahara and H. Akera, this issue, preceding paper, Phys. Rev. B **40**, 11 624 (1989).
[3]W. A. Harrison, Phys. Rev. **123**, 85 (1961).
[4]D. J. Ben Daniel and C. B. Duke, Phys. Rev. **152**, 682 (1966).
[5]G. Bastard, Phys. Rev. B **24**, 5693 (1981); **25**, 7584 (1982).
[6]S. R. White and L. J. Sham, Phys. Rev. Lett. **47**, 879 (1981).
[7]M. Altarelli, Phys. Rev. B **28**, 842 (1983).
[8]See, for example, H. C. Casey, Jr. and M. B. Panish, in *Heterostructure Lasers* (Academic, New York, 1978), Pt. B, p. 17.
[9]See, for example, J. S. Blakemore, J. Appl. Phys. **53**, R123 (1982).
[10]See, for example, H. Kroemer, Surf. Sci. **174**, 299 (1986).
[11]J. P. van der Ziel and A. C. Gossard, Phys. Rev. B **17**, 765 (1978).
[12]A. Ishibashi, Y. Mori, M. Itabashi, and N. Watanabe, J. Appl. Phys. **58**, 2691 (1985).
[13]S. Sasa, K. Kondo, H. Ishikawa, T. Fujii, and S. Muto, Surf. Sci. **174**, 433 (1986).
[14]B. A. Wilson, P. Dawson, C. W. Tu, and R. C. Miller, J. Vac. Sci. Technol. B **4**, 1037 (1986).
[15]K. Yamanaka, T. Fukunaga, N. Tsukada, K. L. I. Kobayashi, and M. Ishii, Appl. Phys. Lett. **48**, 840 (1986).
[16]E. Finkman, M. D. Sturge, and M. C. Tamango, Appl. Phys. Lett. **49**, 1299 (1986).
[17]L. Brey, C. Tejedor, J. L. de Miguel, F. Briones, and K. Ploog, in *Proceedings of the 18th International Conference on the Physics of Semiconductors, Stockholm, 1986,* edited by O. Engström (World Scientific, Singapore, 1987), p. 727.
[18]G. Danan, B. Etienne, F. Mollot, R. Planel, A. M. Jean-Louis, F. Alexandre, B. Jusserand, G. Le Roux, J. Y. Marzin, H. Savary, and B. Sermage, Phys. Rev. B **35**, 6207 (1987).
[19]G. Danan, F. R. Laden, F. Mollot, and R. Planel, Appl. Phys. Lett. **51**, 1605 (1987).
[20]F. Minami, K. Hirata, F. Era, T. Yao, and Y. Masumoto, Phys. Rev. B **36**, 2875 (1987).
[21]D. J. Wolford, T. F. Kuech, J. A. Bradley, M. A. Gell, D. Ninno, and M. Jaros, J. Vac. Sci. Technol. B **4**, 1043 (1986).
[22]M.-H. Meynadier, R. E. Nahory, J. M. Worlock, M. C. Tamargo, J. L. de Miguel, and M. D. Sturge, Phys. Rev. Lett. **60**, 1338 (1988).
[23]E. E. Mendez, E. Calleja, C. E. T. Gonçalves da Silva, L. L. Chang, and W. I. Wang, Phys. Rev. B **33**, 7368 (1986).
[24]E. E. Mendez, E. Calleja, and W. I. Wang, Phys. Rev. B **34**, 6026 (1986).
[25]E. E. Mendez, W. I. Wang, E. Calleja, and C. E. T. Gonçalves da Silva, Appl. Phys. Lett. **50**, 1263 (1987).
[26]A. R. Bonnefoi, T. C. McGill, R. D. Blurnham, and G. B. Anderson, Appl. Phys. Lett. **50**, 344 (1987).
[27]A. R. Bonnefoi, T. C. McGill, and R. D. Blurnham, Phys. Rev. B **37**, 8754 (1988).
[28]P. M. Solomon, S. W. Wright, and D. La Tulipe, Appl. Phys. Lett. **49**, 1453 (1986).
[29]W. E. Pickett, S. G. Louie, and M. L. Cohen, Phys. Rev. B **17**, 815 (1978); J. Vac. Sci. Technol. **15**, 1437 (1978).
[30]J. Sanchez-Dehesa and C. Tejedor, Phys. Rev. B **26**, 5824 (1982).
[31]T. Nakayama and H. Kamimura, J. Phys. Soc. Jpn. **54**, 4726 (1985); H. Kamimura and T. Nakayama, in *Proceedings of the 18th International Conference on the Physics of Semiconductors, Stockholm, 1986,* edited by O. Engström (World Scientific, Singapore, 1987), p. 643; Comments Condensed Matter Phys. **13**, 143 (1987); T. Nakayama, Ph.D. thesis, University of Tokyo, 1987.
[32]D. M. Wood, S.-H. Wei, and A. Zunger, Phys. Rev. Lett. **58**, 1123 (1987).
[33]N. Hamada and S. Ohnishi, Superlatt. Microstruct. **3**, 301 (1987).
[34]E. Caruthers and P. J. Lin-Chung, J. Vac. Sci. Technol. **15**, 1459 (1978).
[35]W. Andreoni and R. Car, Phys. Rev. B **21**, 3334 (1980).
[36]M. Jaros, K. B. Wong, and M. A. Gell, Phys. Rev. B **31**, 1205 (1985); J. Vac. Sci. Technol. B **3**, 1051 (1985).
[37]K. B. Wong, M. Jaros, M. A. Gell, and D. Ninno, J. Phys. C **19**, 53 (1986).
[38]M. A. Gell, D. Ninno, M. Jaros, and D. C. Herbert, Phys. Rev. B **34**, 2416 (1986).
[39]M. G. Gell, D. Ninno, M. Jaros, D. J. Wolford, T. F. Keuch, and J. A. Bradley, Phys. Rev. B **35**, 1196 (1987).
[40]J. N. Schulman and T. C. McGill, Phys. Rev. Lett. **39**, 1680 (1977); Phys. Rev. B **19**, 6341 (1979); **23**, 4149 (1981).
[41]J. N. Schulman and Y.-C. Chang, Phys. Rev. B **24**, 4445 (1981); **27**, 2346 (1983); **31**, 2056 (1985).
[42]Y.-C. Chang and J. N. Schulman, Phys. Rev. B **25**, 3975 (1982); J. Vac. Sci. Technol. **21**, 540 (1982); Phys. Rev. B **31**, 2069 (1985).
[43]D.Z.-Y Ting and Y.-C. Chang, Phys. Rev. B **36**, 4359 (1987).
[44]M. K. Mon, Solid State Commun. **41**, 699 (1982).
[45]E. Yamaguchi, J. Phys. Soc. Jpn. **56**, 2835 (1987).
[46]S. Nara, Jpn. J. Appl. Phys. **26**, 690 (1987); **26**, 1713 (1987).
[47]L. Brey and C. Tejedor, Phys. Rev. B **35**, 9112 (1987).
[48]G. C. Oxbourn and D. L. Smith, J. Vac. Sci. Technol. **16**, 1529 (1979); Phys. Rev. B **19**, 2124 (1979).
[49]G. C. Oxbourn, J. Vac. Sci. Technol. **17**, 1104 (1980); **19**, 592 (1981).
[50]C. Mailhiot, T. C. McGill, and J. N. Schulman, J. Vac. Sci. Technol. B **1**, 439 (1983).
[51]C. Mailhiot, T. C. McGill, and D. L. Smith, J. Vac. Sci. Technol. B **2**, 371 (1984).
[52]A. C. Marsh and J. C. Inkson, Solid State Commun. **52**, 1037 (1984); J. Phys. C **17**, 6561 (1984); **19**, 43 (1986). See also S. Collins, D. Lowe, and J. R. Barker, J. Phys. C **18**, L637 (1985).
[53]A. C. Marsh, Semicond. Sci. Technol. **1**, 32 (1986).
[54]A. C. Marsh and J. C. Inkson, Semicond. Sci. Technol. **1**, 285 (1986); IEEE J. Quantum Electron. **QE-22**, 58 (1986).
[55]D. Y. K. Ko and J. C. Inkson, J. Phys. C **20**, 4213 (1987); Semicond. Sci. Technol. **2**, 442 (1987); **3**, 791 (1988); Phys. Rev. B **38**, 9945 (1988); **38**, 12 416 (1988).
[56]T. Ando and H. Akera, in *Proceedings of the 19th International Conference on Physics of Semiconductors, Warsaw, 1988,* edited by W. Zawadzki (Institute of Physics, Polish Academy of Sciences, Warsaw, 1988), p. 603.
[57]See, for example, A. Pinczuk, S. G. Louie, B. Welber, J. C. Tsang, and J. A. Bradley, in *Physics of Semiconductors, 1978,* edited by B. L. H. Wilson (Institute of Physics, Bristol, 1979), p. 1191, and references cited therein.
[58]D. Bimberg, W. Bludau, R. Linnebach, and E. Bauser, Solid State Commun. **37**, 987 (1981).
[59]J. M. Luttinger and W. Kohn, Phys. Rev. **97**, 869 (1955).
[60]H. Akera, S. Wakahara, and T. Ando, Surf. Sci. **196**, 694 (1988).
[61]D. J. Chadi and M. L. Cohen, Phys. Status Solidi B **68**, 405 (1975).
[62]See, for example, L. D. Landau and E. M. Lifshitz, in *Quantum Mechanics* (Pergamon, Oxford, 1977), pp. 55ff.

[63]P. J. Price, Surf. Sci. **196**, 394 (1988).
[64]H. Akera and T. Ando, Phys. Rev. B **40**, 2914 (1989).
[65]R. Dingle, *Festkörperprobleme* (*Advances in Solid State Physics*), edited by P. Grosse (Pergamon, Braunschweig, 1975), Vol. XV, p. 21.
[66]R. C. Miller, A. C. Gossard, D. A. Kleinman, and O. Munteanu, Phys. Rev. B **29**, 3470 (1984).
[67]G. Bastard, Phys. Rev. B **24**, 5693 (1981).
[68]M. Tsuchiya and H. Sakaki, Appl. Phys. Lett. **49**, 88 (1986).